January 1, 2006

# Theoretical Analysis of the Effect of Insoluble Surfactant on the Dip Coating of Chemically Micropatterned Surfaces

N Tiwari
JM Davis

# Theoretical analysis of the effect of insoluble surfactant on the dip coating of chemically micropatterned surfaces

Naveen Tiwari and Jeffrey M. Davis

Citation: Physics of Fluids (1994-present) **18**, 022102 (2006); doi: 10.1063/1.2171715
View online: http://dx.doi.org/10.1063/1.2171715
View Table of Contents: http://scitation.aip.org/content/aip/journal/pof2/18/2?ver=pdfcov
Published by the AIP Publishing

# Theoretical analysis of the effect of insoluble surfactant on the dip coating of chemically micropatterned surfaces

Naveen Tiwari and Jeffrey M. Davis[a)]
*Department of Chemical Engineering, University of Massachusetts, Amherst, Massachusetts 01003*

(Received 1 June 2005; accepted 9 January 2006; published online 10 February 2006)

Microfluidic flow on chemically heterogeneous surfaces is a useful technique with applications ranging from selective material deposition to the self-assembly of nanostructures. The recent theoretical analysis by Davis [Phys. Fluids **17**, 038101 (2005)] of the dip coating of a pure fluid onto vertical, wetting stripes surrounded by nonwetting regions quantified the experimentally observed deviations from the classical Landau-Levich result due to lateral confinement of the fluid by chemical surface patterning. In this present work, the analysis of dip coating of these heterogeneous surfaces is extended to a liquid containing an insoluble surfactant. Using matched asymptotic expansions based on lubrication theory in the limit of a small capillary number, the thickness of the deposited liquid film and the surfactant concentration in the deposited monolayer are predicted for a wide range of fluid properties and process parameters. The increase in the deposited film thickness is shown analytically to be limited by a multiplicative factor of $4^{1/3}$ times the result for a pure liquid. Numerical results demonstrate that the thickening due to Marangoni effects is nonmonotonic in the capillary number because of the competition between viscous stresses, Marangoni stresses, and surface diffusion. © *2006 American Institute of Physics*.
[DOI: 10.1063/1.2171715]

## I. INTRODUCTION

Free-surface microfluidic flow on heterogeneous surfaces has numerous applications in current micro- and nanotechnology research, including selective inking,[1] sol-gel processing,[2] patterned colloidal deposition,[3] fabrication of organic thin-film transistors and inorganic thin films,[4,5] and controlling deposition in the self-assembly of hierarchically organized structures[5,6] and carbon nanotube arrays.[7,8] These patterned surfaces may also facilitate the reproducible growth of ordered arrays of nanoparticles and nanowires.[9,10] One of the most simple and important techniques used to coat fluid onto a surface is dip coating, which has been extensively investigated both experimentally and theoretically for chemically homogeneous plates, rods, and fibers.[2,11–18] Landau and Levich[11] first derived an expression for the deposited liquid film thickness, $h_\infty$, on a flat and homogeneous substrate withdrawn at velocity $U$ from a bath of liquid with density $\rho$, viscosity $\mu$, and surface tension $\sigma_0$,

$$h_\infty = 0.946\sqrt{\frac{\sigma_0}{\rho g}}\mathrm{Ca}^{2/3}, \tag{1}$$

where $g$ is the gravitational acceleration, $\mathrm{Ca}=\mu U/\sigma_0$ is the capillary number, and $L_c \equiv (\sigma_0/\rho g)^{1/2}$ is the capillary length of the liquid. Wilson[15] later used a more formal analysis based on matched asymptotic expansions to derive an $O(\mathrm{Ca})$ correction term.

More recently, as microfabrication has become common and microfluidic applications have increased, the dip coating technique has been used to achieve selective material deposition on micropatterned surfaces.[1,3,5,6] Davis[19] performed the first theoretical analysis of the dip coating of vertical, wetting stripes of width $\widetilde{W}$ on an otherwise nonwetting, planar surface using a matched asymptotic analysis. For sufficiently narrow stripes ($\rho g \widetilde{W}^2/\sigma_0 \ll 1$), he derived an equation for the centerline thickness of the liquid film entrained on the wetting stripes,[19]

$$h_\infty = 0.356\widetilde{W}\,\mathrm{Ca}^{1/3}. \tag{2}$$

The fluid confinement by chemical surface patterning strongly affects the thickness of the entrained liquid film, as the characteristic length scale is reduced from the $O$(mm) capillary length to the $O(\mu\mathrm{m})$ stripe width by the effect of fluid confinement on the curvature of the meniscus near the liquid bath. The exponent of the capillary number decreases from 2/3 to 1/3 as a result of the streamwise change in the transverse curvature of the free surface along the stripe, which modifies the asymptotic matching process. This result is within about one percent of experimental measurements.[1]

Many applications on heterogeneous surfaces involve the presence of surfactants, either as integral components of the process or through contamination of the liquid. A nonuniform distribution of surfactants can induce Marangoni stresses at the free surface, which can significantly modify the coating dynamics and thickness of the entrained film. While these effects have been quantified for the dip coating of homogeneous plates,[20] Marangoni drying,[21,22] and the related problem of bubble motion in capillary tubes,[23,24] they have not been analyzed for heterogeneous substrates.

In the present work we focus on the dip coating of a liquid containing an insoluble surfactant onto a chemically micropatterned, planar surface, as shown schematically in Fig. 1. As the plate is withdrawn from the bath, liquid is

a)Electronic mail: jmdavis@ecs.umass.edu

 

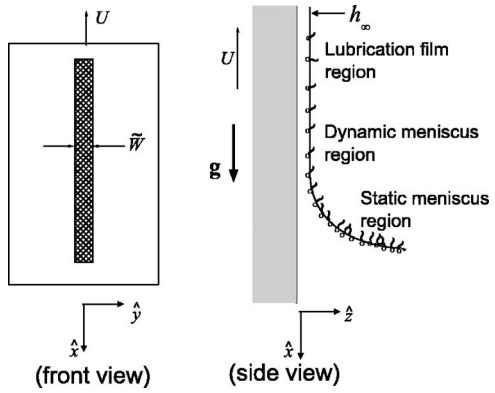


FIG. 1. Schematic diagram showing the dip coating of a liquid containing an insoluble surfactant onto a wetting microstripe. The planar surface surrounding the microstripe is nonwetting.

entrained on the wetting stripe(s), and no liquid is entrained on the surrounding nonwetting regions. A matched asymptotic analysis is used to explore the effect of stripe width, capillary number, and Marangoni number on the thickness of the entrained liquid film and the surface concentration of the entrained surfactant monolayer. The governing equations are derived from simplification of the Navier-Stokes equations in Sec. II. The appropriate scalings and numerical techniques are presented in Sec. III. Numerical results are presented in Sec. IV and are analyzed and compared to earlier work in Sec. V.

## II. GOVERNING EQUATIONS

Consider the steady-state dip coating of a solution containing insoluble surfactant onto a planar, nonwetting substrate containing a vertical, wetting microstripe of width $\tilde{W}$ that is withdrawn at constant velocity $U$ in the negative $x$ direction, from a solution containing insoluble surfactant, as shown in Fig. 1. The coordinate $z$ is directed outwardly normal from the substrate. (The analysis is analogous for a parallel array of wetting microstripes.) The fluid has kinematic viscosity $\nu$ and surface tension $\sigma$ that varies with the local surfactant concentration. As the plate is withdrawn, a thin liquid film is entrained along the wetting stripe, and no liquid is entrained on the surrounding nonwetting regions. There is no flow in the $y$ direction along the microstripe due to symmetry and the transverse confinement of fluid by the chemical surface patterning. The governing equations are the steady-state momentum balance,

$$\hat{\boldsymbol{u}} \cdot \boldsymbol{\nabla} \hat{\boldsymbol{u}} = \frac{-1}{\rho} \nabla \hat{p} + \nu \nabla^2 \hat{\boldsymbol{u}} + \boldsymbol{g}, \tag{3}$$

and the continuity equation for an incompressible fluid,

$$\boldsymbol{\nabla} \cdot \hat{\boldsymbol{u}} = 0, \tag{4}$$

where $\hat{\boldsymbol{u}}$ is the fluid velocity.

At $\hat{z}=0$, the boundary conditions are no slip and no penetration at the plate surface,

$$\hat{\boldsymbol{u}} = -U\boldsymbol{e}_x. \tag{5}$$

At the free surface, $\hat{z}=\hat{h}(\hat{x},\hat{y})$, the kinematic condition,

$$\boldsymbol{n} \cdot \hat{\boldsymbol{u}} = 0, \tag{6}$$

and the normal and tangential stress balances,

$$\boldsymbol{n} \cdot \mathbf{T} \cdot \boldsymbol{n} = \sigma(\boldsymbol{\nabla}_s \cdot \boldsymbol{n}), \tag{7}$$

$$\boldsymbol{t} \cdot \mathbf{T} \cdot \boldsymbol{n} = -\boldsymbol{t} \cdot \boldsymbol{\nabla}_s(\sigma), \tag{8}$$

are enforced. Here, $\boldsymbol{n}$ and $\boldsymbol{t}$ are the normal and tangential unit vectors to the free surface, respectively, $\mathbf{T}$ is the total stress tensor, and $\boldsymbol{\nabla}_s$ is the surface gradient operator.

The equations of motion are coupled to a mass balance for the insoluble surfactant, which determines the shear stress induced by the surface gradient in surface tension in the tangential stress balance,

$$\frac{\partial \hat{\Gamma}}{\partial t} + \boldsymbol{\nabla}_s \cdot (\hat{\Gamma} \hat{\boldsymbol{u}}_s) = D_s \nabla_s^2 \hat{\Gamma} + j, \tag{9}$$

where $\hat{\Gamma}$ is the surface concentration of the insoluble surfactant, $\hat{\boldsymbol{u}}_s$ is the surface velocity vector, $D_s$ denotes the surface diffusivity of the surfactant, and $j$ is the net flux from the bulk phase to the surface. Because of the restriction that the surfactant is insoluble in the bulk liquid, $j=0$ in what follows.

In the following analysis, a linear equation of state is used for the variation of surface tension with surfactant concentration. This approximation is generally accurate if the surface concentration or its spatial variation is small or if the surfactant follows the Gibbs surface equation of state, even for concentrated monolayers. The surface tension is then related to the surfactant concentration by

$$\sigma = \sigma_0 + \left( \frac{\partial \sigma}{\partial \hat{\Gamma}} \right)_{\hat{\Gamma}_0} (\hat{\Gamma} - \hat{\Gamma}_0), \tag{10}$$

where $\hat{\Gamma}_0$ is the surface concentration on the surface of the bulk liquid near the meniscus and $\sigma_0$ is the surface tension at that concentration. (It is straightforward to incorporate more complex equations of state into the following analysis.) It is assumed in the analysis that $\hat{\Gamma}_0$ remains constant throughout the coating process.

This analysis is restricted to small capillary numbers, $\mathrm{Ca} \equiv \mu U/\sigma_0 \ll 1$, which is relevant to the experimental conditions used for many applications on micropatterned surfaces. This restriction also makes the viscous contributions to the normal stress balance negligible, which allows for a more tractable analysis. Because $\mathrm{Ca} \ll 1$, an $\hat{x}=$const cross section of the free surface of the liquid along the stripe must be an arc of a circle,[19] which within the lubrication approximation simplifies to a parabolic cap. The introduction of $\hat{h}(\hat{x},\hat{y}) = \hat{h}(\hat{x})[1-4(\hat{y}/\tilde{W})^2]$ reduces the analysis to a one-dimensional asymptotic matching problem for the entrained film thickness at the centerline of the stripe, $\hat{h}(\hat{x}) \equiv \hat{h}(\hat{x},\hat{y}=0)$. At the centerline of the stripe ($\hat{y}=0$), symmetry requires that $\hat{h}_{\hat{y}}=0$, $\hat{\boldsymbol{u}}_{\hat{y}}=\boldsymbol{0}$, and $\hat{p}_{\hat{y}}=0$. From here on, $\hat{h}$ refers to the dimensional film thickness along the centerline of the stripe and hence depends only on $\hat{x}$. Using $W$ ($\equiv \tilde{W}/\sqrt{8}$), $U$, $\sigma_0$, and $\hat{\Gamma}_0$ as the scales for length, velocity, surface tension, and

surface concentration, respectively, and evaluating at $\hat{y}=0$, Eqs. (3)–(9) are rewritten in dimensionless form as

$$u_x + v_z = 0, \tag{11}$$

$$\mathrm{Re}(uu_x + vu_z) = -\frac{\partial P}{\partial x} + \mathrm{Bo}\,\mathrm{Ca}^{-1} + u_{xx} + u_{zz}, \tag{12}$$

$$\mathrm{Re}(uv_x + vv_z) = -\frac{\partial P}{\partial z} + v_{xx} + v_{zz}, \tag{13}$$

where $\mathrm{Re} \equiv WU/\nu$ is the Reynolds number.

At $z=0$, the no slip condition is

$$u = -1, \tag{14}$$

and the no penetration condition is

$$v = 0. \tag{15}$$

At $z=h(x)$, the kinematic condition reduces to

$$v - h_x u = 0. \tag{16}$$

The normal stress balance is

$$P + \frac{2}{(1+h_x^2)}[h_x(u_z + v_x) - h_x^2 u_x - v_z] = -(\mathrm{Ca}^{-1})(1 - \mathrm{M}\Gamma)(2\kappa), \tag{17}$$

and the tangential stress balance is

$$\mathrm{Ca}[(u_z + v_x)(1 - h_x^2) + 2h_x(v_z - u_x)] = -\mathrm{M}(1+h_x^2)^{1/2}\Gamma_x. \tag{18}$$

The dimensionless surfactant mass balance is

$$[(1+\Gamma)u_s]_x + h_x[(1+\Gamma)h_x u_s]_x = \frac{1}{\mathrm{Pe}}\left(\Gamma_{xx} - \frac{h_x h_{xx}\Gamma_x}{(1+h_x^2)}\right), \tag{19}$$

where $u$ and $v$ are the velocity components in $x$ and $z$ directions, respectively, $u_s \equiv u(x, z=h)$ is the surface velocity in the $x$ direction, and $P$ is the rescaled pressure.

The dimensionless surface concentration $\Gamma$, capillary number Ca, Bond number Bo, Marangoni number M, and Peclet number Pe are then defined as

$$\Gamma = \left(\frac{\hat{\Gamma} - \hat{\Gamma}_0}{\hat{\Gamma}_0}\right), \quad \mathrm{Ca} = \left(\frac{\mu U}{\sigma_0}\right), \quad \mathrm{Bo} = \left(\frac{\rho g W^2}{\sigma_0}\right),$$

$$\mathrm{M} = -\frac{\hat{\Gamma}_0}{\sigma_0}\left(\frac{\partial \sigma}{\partial \hat{\Gamma}}\right)_{\hat{\Gamma}_0}, \quad \mathrm{Pe} = \left(\frac{UW}{D_s}\right). \tag{20}$$

Note that $-1 \leqslant \Gamma \leqslant 0$ because of the definition of the dimensionless concentration, $\Gamma$.

## III. FLOW REGIONS AND ASYMPTOTIC ANALYSIS

The coating flow can be divided into three regions (shown in Fig. 1) based on the relative importance of the governing forces. Far above the liquid reservoir, as $x \to -\infty$, is the constant film thickness region in which the desired film has been achieved and the streamwise gradients in the film thickness and surfactant concentration vanish. Near the liquid bath is the static meniscus, in which there is a balance between the capillary forces from the streamwise and transverse curvature of the free surface. Between these two regions is the dynamic meniscus, or overlap region, in which viscous and capillary forces balance. The lubrication approximation is applied to derive the governing equations in this region, and the solution must smoothly match the limiting behavior of the thin film and static meniscus regions. The simplified governing equations can be solved far above the liquid reservoir (in terms of the unknown constant film thickness and surfactant concentration) and where the plate meets the liquid reservoir (static meniscus). Asymptotic matching in the dynamic meniscus can then be used to determine the entrained film thickness, $h_\infty$, and surfactant concentration in the entrained film, $\hat{\Gamma}_c$.

The lateral fluid confinement by chemical surface patterning induces a significant transverse curvature of the free surface. This curvature causes two key differences between this analysis on micropatterned surfaces and the conventional analysis[20] on uniform surfaces. In the static meniscus, the streamwise curvature is balanced by the transverse curvature, and gravity is negligible to leading order for the narrow stripes considered. On uniform surfaces, however, the streamwise curvature is balanced by gravity, which leads to a different asymptotic matching condition in the dynamic meniscus than for the patterned surface. In addition, the transverse curvature in the dynamic meniscus for patterned surfaces adds a term to the capillary pressure [Eq. (30)] and modifies the asymptotic matching [Eq. (38)], as explained in more detail below.

### A. Dynamic meniscus

Appropriate rescaling of the equations of motion in the dynamic meniscus is accomplished by retaining $W$ as the scale in the $x$ direction to balance the transverse curvature due to chemical confinement with the streamwise curvature along the stripes. All the variables in the $z$ direction are rescaled with $\mathrm{Ca}^{1/3}$ to balance the capillary forces with viscous forces. The rescaled variables are then defined as

$$\bar{x} = x, \quad \bar{y} = y, \quad \bar{z} = \left(\frac{z}{\mathrm{Ca}^{1/3}}\right),$$

$$\bar{u} = u, \quad \bar{v} = \left(\frac{v}{\mathrm{Ca}^{1/3}}\right),$$

$$\bar{P} = P\,\mathrm{Ca}^{2/3}, \quad \bar{h} = \left(\frac{h}{\mathrm{Ca}^{1/3}}\right), \tag{21}$$

$$\bar{\Gamma} = \Gamma, \quad \bar{\mathrm{M}} = \left(\frac{\mathrm{M}}{\mathrm{Ca}^{2/3}}\right), \quad \bar{D} = \mathrm{Pe}.$$

After rescaling in the dynamic meniscus and at leading order, Eqs. (11)–(13) reduce to

$$\bar{u}_{\bar{x}} + \bar{v}_{\bar{z}} = 0, \tag{22}$$

$$-\bar{P}_{\bar{x}}+\bar{u}_{\bar{z}\bar{z}}=0, \tag{23}$$

$$\bar{P}_{\bar{z}}=0. \tag{24}$$

The no-slip, no-penetration, and kinematic conditions remain: at $\bar{z}=0$,

$$\bar{u}=-1, \tag{25}$$

$$\bar{v}=0, \tag{26}$$

and at $\bar{z}=\bar{h}$,

$$\bar{v}-\bar{h}_{\bar{x}}\bar{u}=0. \tag{27}$$

The normal and tangential stress balances at $\bar{z}=\bar{h}$, Eqs. (17) and (18) become

$$\bar{P}=-(2\bar{\kappa})(1-\mathrm{M}\bar{\Gamma}), \tag{28}$$

$$\bar{u}_{\bar{z}}=-\bar{\mathrm{M}}\bar{\Gamma}_{\bar{x}}. \tag{29}$$

With $\mathrm{Ca}^{2/3}\ll 1$, the dimensionless curvature reduces to $2\bar{\kappa}\approx\bar{h}_{\bar{x}\bar{x}}+\bar{h}_{\bar{y}\bar{y}}$. As the film profile can be reduced to $\bar{h}(\bar{x},\bar{y})=\bar{h}(\bar{x})[1-\bar{y}^2/2]$ along $\bar{y}=0$, as discussed in the previous section, $\bar{h}_{\bar{y}\bar{y}}(\bar{y}=0)=-\bar{h}(\bar{x})$. The curvature in Eq. (28) therefore reduces to $2\bar{\kappa}=\bar{h}_{\bar{x}\bar{x}}-\bar{h}$, and the rescaled normal stress balance simplifies to

$$\bar{P}=-(\bar{h}_{\bar{x}\bar{x}}-\bar{h})(1-\mathrm{M}\bar{\Gamma}). \tag{30}$$

Note that on uniform surfaces, $\bar{h}_{\bar{x}\bar{x}}-\bar{h}$ in Eq. (30) is simply replaced by $\bar{h}_{\bar{x}\bar{x}}$ because there is no transverse curvature of the free surface. Finally, the rescaled mass balance for the surfactant, Eq. (19), becomes

$$[(1+\bar{\Gamma})\bar{u}_s]_{\bar{x}}=\frac{1}{\mathrm{Pe}}\bar{\Gamma}_{\bar{x}\bar{x}}. \tag{31}$$

The lubrication condition required for these simplifications is then $\mathrm{Re}\,\mathrm{Ca}^{2/3}\ll 1$. In Eq. (23), it is assumed that gravity is negligible relative to the viscous forces. This constraint requires $\mathrm{Bo}\,\mathrm{Ca}^{-1/3}\ll 1$, which reduces to $W^2\ll L_c^2\,\mathrm{Ca}^{1/3}$. This restriction provides an upper bound for the width of the stripe for which this assumption and hence the analysis is valid. Note also that the viscous contributions to the normal stress balance can be neglected because $\mathrm{Ca}\ll 1$. In Eq. (29), the leading-order tangential stress term balances the Marangoni stress, and in Eq. (31) the leading-order convection term balances the diffusion term.

These equations are solved by substituting Eq. (30) into Eq. (23), integrating with respect to $\bar{z}$, and using Eqs. (25) and (29) to solve for $\bar{u}$. Then the flow rate in the lubrication region is equated to the flow rate in the constant film region to give two coupled differential equations in $\bar{h}$ and $\bar{\Gamma}$:

$$(\bar{h}_{\bar{x}\bar{x}\bar{x}}-\bar{h}_{\bar{x}})=\frac{1}{(1-\mathrm{M}\bar{\Gamma})}\left(\frac{3(\bar{h}-\bar{h}_\infty)}{\bar{h}^3}+\frac{3\bar{\mathrm{M}}\bar{\Gamma}_{\bar{x}}}{2\bar{h}}+(\bar{h}_{\bar{x}\bar{x}}-\bar{h})\times(\mathrm{M}\bar{\Gamma}_{\bar{x}})\right), \tag{32}$$

$$\bar{\Gamma}_{\bar{x}}=\frac{2\bar{D}[(1+\bar{\Gamma})(\bar{h}-3\bar{h}_\infty)+2\bar{h}(\bar{\Gamma}_c+1)]}{\bar{h}[4+\bar{\mathrm{M}}\bar{D}\bar{h}(1+\bar{\Gamma})]}. \tag{33}$$

### B. Lubrication film

As $\bar{x}\to-\infty$, the constant film thickness region is approached, and the solution is

$$\bar{u}=-1, \quad \forall\,\bar{z}, \tag{34}$$

$$\bar{\Gamma}\to\bar{\Gamma}_c, \tag{35}$$

$$\bar{h}\to\bar{h}_\infty. \tag{36}$$

### C. Static meniscus

In the meniscus region, $W$ is the appropriate length scale for all coordinates, which is analogous to the use of the cylinder radius to scale both coordinates in the outer region for the determination of the shape of a static meniscus on a thin cylinder.[25,26] With these scaled variables, the curvature in the static meniscus is given by

$$h^3\frac{\partial(2\kappa)}{\partial x}=\mathrm{Ca}(h-h_\infty)+\mathrm{Bo}(h_\infty^3-h^3). \tag{37}$$

Because of the previously mentioned constraints on Ca and Bo, the static meniscus is not influenced by the motion of the plate or by gravity at leading order. Also, in this static meniscus region, for $\mathrm{Bo}\ll 1$, the liquid-vapor interface within several stripe widths of the wall is a minimal surface with zero mean curvature ($2\kappa=0$).[19] In order to neglect gravity in Eq. (23), it was required that $\mathrm{Bo}\ll\mathrm{Ca}^{1/3}$. With $\mathrm{Ca}\ll 1$, the terms of $O(\mathrm{Bo})$ are uniformly negligible, and corrections to the shape of the meniscus due to the inclusion of the gravity are insignificant. The mean curvature in the static meniscus region therefore reduces to $2\kappa=0$, and the exact meniscus profile need not be determined explicitly.[19] Evaluating $2\kappa$ along the centerline of the stripe ($y=0$) and noting that the free surface must be symmetric (and that $h_x\to 0$ at the top of the static meniscus to match the dynamic meniscus) reveals that $h_{xx}+h_{yy}\to 0$ is the desired limiting behavior at the top of the static meniscus to which the solution in the dynamic meniscus should be matched. For the surfactant concentration, $\hat{\Gamma}\to\hat{\Gamma}_0$.

In the scaled variables of the transition/overlap region, these asymptotic constraints reduce to

$$\bar{h}_{\bar{x}\bar{x}}-\bar{h}\to 0, \tag{38}$$

$$\bar{\Gamma} \to 0, \tag{39}$$

as $\bar{x} \to \infty$.

### D. Numerical solution

Equations (32) and (33) were solved via a shooting method shown to be effective for similar thin film equations.[27,28] The MATLAB 6.1 functions *ode45* and *ode23s* were used for the numerical integration. Integration begins in the constant film thickness region (as $x \to -\infty$), with linearization of Eqs. (32) and (33) about the solution given by Eqs. (35) and (36) used to obtain the initial conditions for the integration in terms of the unknown constants $\bar{h}_\infty$ and $\bar{\Gamma}_c$ and a small shooting parameter $\epsilon \ll 1$. The value of $\epsilon$ was typically $O(10^{-6})$ for the computations. The resulting initial value problems were integrated to the static meniscus region ($x \to \infty$) until $\bar{h}_{\bar{x}\bar{x}} - \bar{h}$ and $\bar{\Gamma}$ reached their constant, limiting values. If the matching conditions given by Eqs. (38) and (39) were not satisfied, the guesses for $\bar{h}_\infty$ and $\bar{\Gamma}_c$ were refined simultaneously using the Newton-Raphson method. An error tolerance of $10^{-10}$ was used to determine if the matching conditions were met.

## IV. RESULTS

This analysis predicts that the dimensional entrained film thickness is given by

$$\hat{h}_\infty = \bar{h}_\infty W \, \mathrm{Ca}^{1/3}. \tag{40}$$

For $\mathrm{M}=0$, $\bar{h}_\infty = 1.008\,29$, which recovers the recent prediction by Davis[19] for a pure liquid and provides the lower bound for the thickness of the entrained film on a chemically micropatterned surface. If $\mathrm{M} \neq 0$, then $\bar{h}_\infty = \bar{h}_\infty(\mathrm{M}, \mathrm{Ca})$, and exact power-law behavior is not observed. In this section, numerical results are reported for values of the rescaled stripe width ($W$) ranging from 1 to 100 $\mu$m. A wide range of values was chosen for the Marangoni factor (M) based on experimental data for common fluids.[29] To cover a range of fluids and different withdrawal velocities, the range $10^{-11} \leqslant \mathrm{Ca} \leqslant 10^{-2}$ was investigated. (This analysis does not take into account disjoining pressure effects, which may become important for very small values of the capillary number or stripe width, which correspond to very thin films.) Unless otherwise specified, it was assumed that $D_s = 10^{-9}$ m/s$^2$ in all computations. Note that varying the rescaled stripe width, $W$, is equivalent to varying the surface diffusivity, $D_s$, because these parameters appear in the surface Péclet number, Pe, and thus are important only as the ratio $D_s/W$. (The effect of withdrawal velocity is independently specified via the capillary number.) For $D_s = 0$, all effects of $W$ are encompassed in the scaling without the introduction of dimensionless parameters, so the dimensionless results become independent of $W$ and collapse onto one curve (for each M), as shown in Fig. 2. The decrease in the numerical prefactor with increasing Ca is due to the increase in viscous stress, which overcomes the surface dilation caused by the Marangoni stress. As M is increased, the Marangoni stress becomes more significant, and the decrease in the numerical prefactor due to the increase in viscous stress becomes very small.

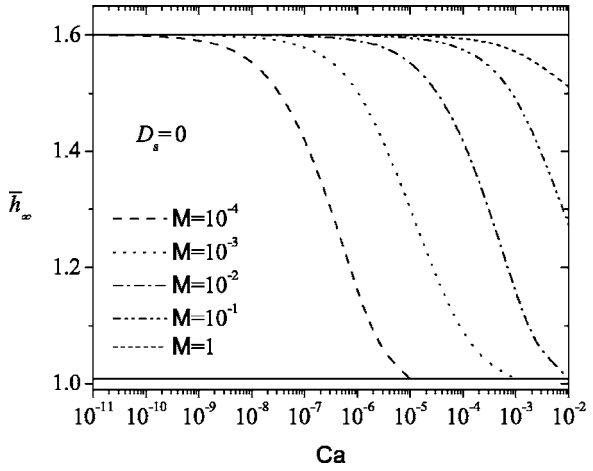


FIG. 2. Dimensionless entrained film thickness $\bar{h}_\infty$ vs Ca for the case $D_s = 0$.

The variation of $\bar{h}_\infty$ with Ca for various M and $W$ (with $D_s \neq 0$) is shown in Fig. 3. The presence of insoluble surfactant, which corresponds to nonzero M, has a thickening effect on the entrained film, which was also found for a homogeneous substrate.[20] As noted by Davis,[19] the effect of the transverse curvature of the free surface due to fluid confinement is observed in the characteristic length scale and prefactor of the capillary number in Eq. (40). The dependence of $\bar{h}_\infty$ on Ca is qualitatively similar for different values of $W$, but the curves shift upward as $W$ increases. This shift is more significant for smaller values of M, but for larger M all curves tend to reach to the maximum limit of the entrained film thickness, about which details are given in Sec. IV A. For fixed $U$ and $D_s \neq 0$, an increase in $W$ corresponds to an increase in the surface Péclet number, which translates into a diminished influence of surface diffusion relative to convection. The resulting surfactant concentration profile becomes steeper, thereby inducing a larger Marangoni stress that leads to film thickening.

The dimensionless concentration in the entrained film versus capillary number for different values of M is shown in Fig. 4. Because of the definition of $\Gamma$ in Eq. (20), the dimensionless surfactant concentration corresponds to the difference in surfactant concentration between the entrained film and the meniscus. The dimensional surfactant concentration is given by $\hat{\Gamma} = \hat{\Gamma}_0(\Gamma + 1)$, so $\Gamma_c = 0$ corresponds to the same surfactant concentration in the entrained film as the meniscus, while $\Gamma_c = -1$ corresponds to no surfactant on the entrained film.

The effects of M on the plots in Figs. 3 and 4 are related. As M increases in Fig. 3, the thickness of the entrained film increases. Correspondingly, as M increases in Fig. 4, the dimensionless concentration increases for a particular value of Ca, corresponding to an increase in the amount of surfactant present in the entrained film. As M is increased for fixed Ca, the Marangoni stress induces a surface velocity that results in a larger concentration of surfactant in the entrained film. As

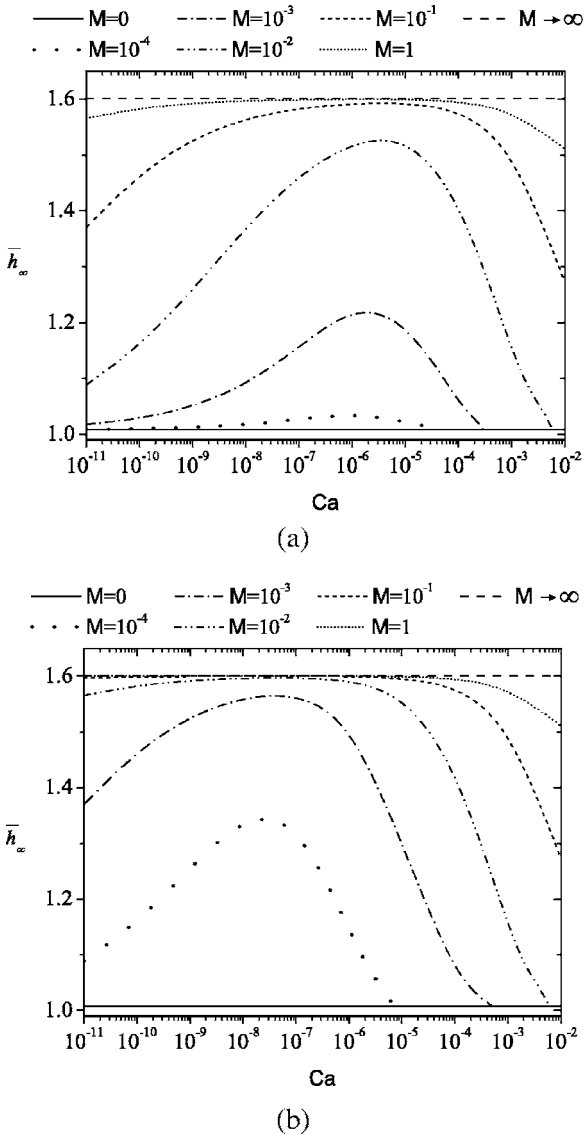


FIG. 3. Dimensionless entrained film thickness $\bar{h}_\infty$ vs Ca for (a) $W=1$ $\mu$m and (b) $W=100$ $\mu$m.

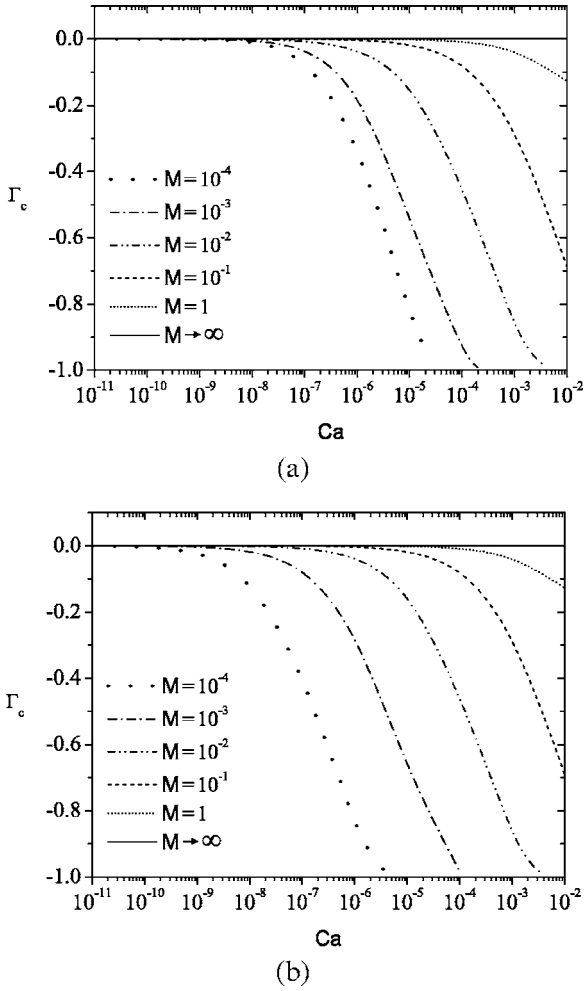


FIG. 4. Dimensionless surface concentration of surfactant in the entrained film ($\Gamma_c$) vs Ca for (a) $W=1$ $\mu$m, and (b) $W=100$ $\mu$m. The value ($\Gamma_c$)=0 corresponds to the same surfactant concentration in the deposited film and liquid reservoir, while ($\Gamma_c$)=−1 corresponds to no surfactant in the deposited film.

$W$ is increased, the Péclet number increases, which corresponds to an increase in convection relative to diffusion. The concentration of the surfactant therefore decreases in the entrained film, which is clearly indicated by the downward shift of the curves in Figs. 4(a)–4(c) for a fixed value of M. As M becomes very large, the concentration profile is essentially independent of Ca. These large values of M correspond to cases in which the maximum increase in film thickness is attained, which is discussed further in Sec. IV A.

To demonstrate the effect of stripe width (equivalently, $D_s$) on the coating process more clearly, the entrained film thickness is plotted versus $W$ for selected values of the capillary number in Fig. 5. Note that this change in the dimensionless entrained film thickness occurs because surface diffusion becomes less important relative to convection as $W$ increases for fixed $U$ and $D_s$ (corresponding to an increase in $\bar{D}$). As the capillary number increases to $\mathrm{Ca}=10^{-2}$, $\bar{h}_\infty$ becomes independent of $W$ for all values of M. At such relatively large Ca, convection dominates diffusion, and the results correspond to those obtained in Fig. 2 for $\bar{D}\to\infty$. The dimensionless results also become independent of $W$ for all Ca as $D_s\to 0$ ($\bar{D}\to\infty$), as shown earlier in Fig. 2.

The corresponding plots of surfactant concentration versus stripe width for different values of M are shown in Fig. 6. The curves show a decrease in the dimensionless concentration and hence a decrease in the surfactant concentration in the entrained film with an increase in $W$. This curve also flattens out for very large values of M, which corresponds to the case of maximum film thickness. The trends for a fixed value of Ca can again be explained on the basis of increased convection relative to surface diffusion with increased $W$, which is responsible for the decrease in surfactant concentration in the film at higher values of $W$. As Ca is increased, convection dominates, and the surfactant concentration remains the same for all values of $W$.

### A. Maximum increase in entrained film thickness

The increase in $\bar{h}_\infty$ with M is found to be limited by a maximum factor beyond which an increase in M has no fur-

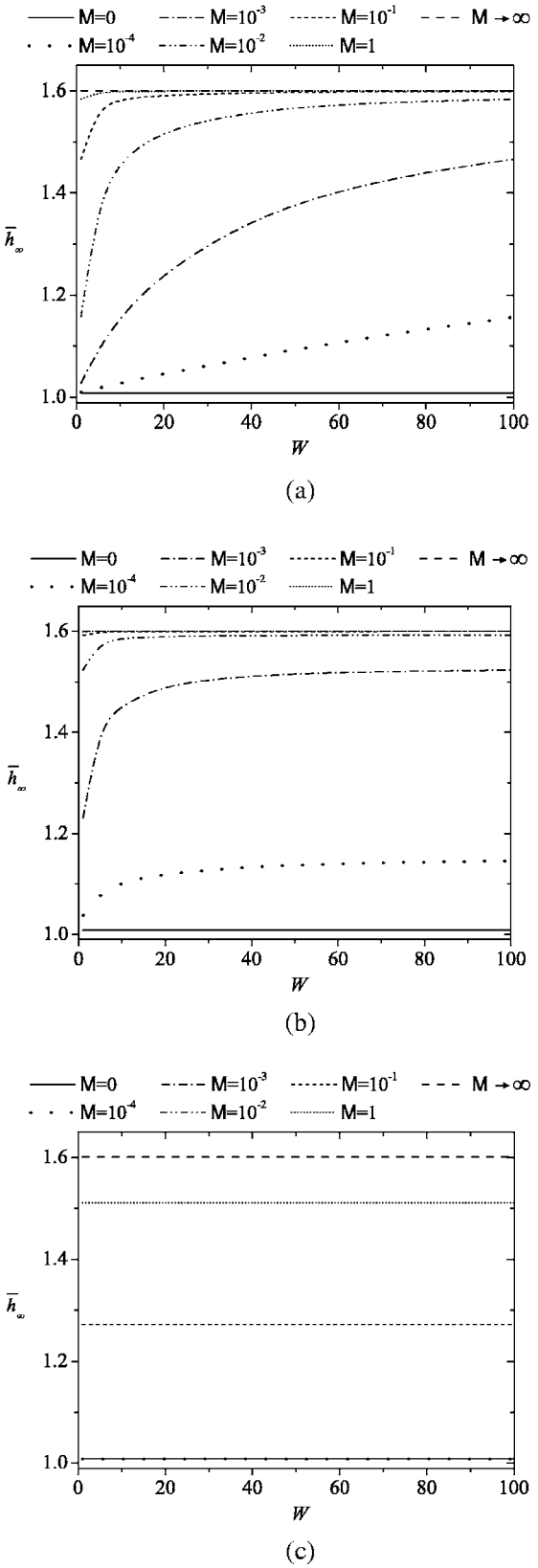


FIG. 5. Dimensionless entrained film thickness $\bar{h}_\infty$ vs $W$ ($\mu$m) for (a) Ca $=10^{-10}$, (b) Ca$=10^{-6}$, and (c) Ca$=10^{-2}$.

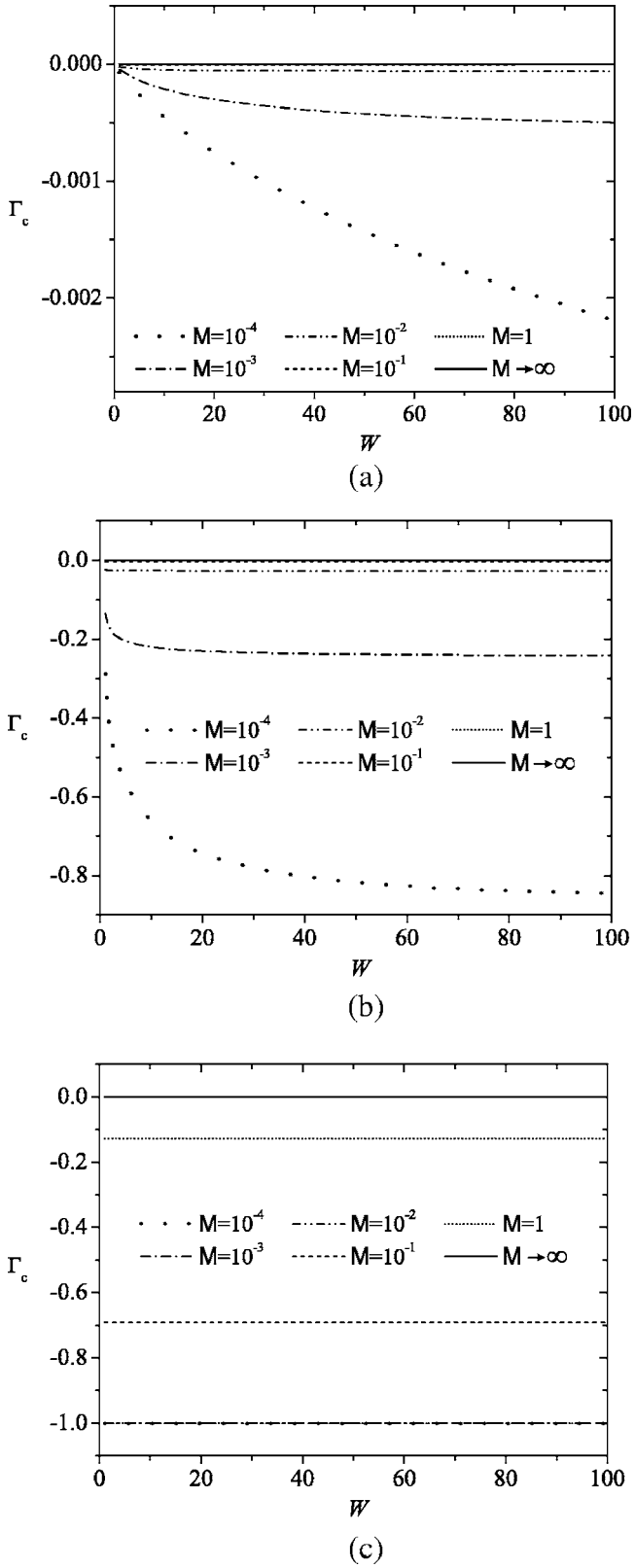


FIG. 6. Dimensionless surface concentration of surfactant in the entrained film ($\Gamma_c$) vs $W$ ($\mu$m) for (a) Ca$=10^{-10}$, (b) Ca$=10^{-6}$, (c) Ca$=10^{-2}$.

ther effect, which is analogous to results for dip coating of uniform surface[20] and the motion of a bubble in a capillary tube.[24] As $\bar{M}\to\infty$, the dimensionless entrained film thickness approaches a value of 1.600 56, which is exactly $4^{1/3}$ times the value of the dimensionless entrained film thickness for the base case (M$=0$). This can be easily shown by applying the limit $\bar{M}\to\infty$ first to Eq. (33), which shows that $\bar{\Gamma}_{\bar{x}}=\bar{\Gamma}=0$ (but $\bar{M}\bar{\Gamma}_{\bar{x}}$ is finite). Taking the limit of Eq. (32) as $\bar{M}\to\infty$ then yields

$$(\bar{h}_{\bar{x}\bar{x}\bar{x}} - \bar{h}_{\bar{x}}) = \frac{12(\bar{h} - \bar{h}_\infty)}{\bar{h}^3}. \tag{41}$$

The initial conditions and the matching conditions remain the same as in the previous cases. Note that Eq. (41) reduces to Eq. (32) for $\mathsf{M}=0$ with the rescaling $\hat{h}=4^{-1/3}\bar{h}$, so $\bar{h}_\infty = 4^{1/3}\hat{h}_\infty$, with $\hat{h}_\infty = 1.008\ 29$. The same maximum limit of $4^{1/3}$ times the result for $\mathsf{M}=0$ was also found from the numerical results. The maximum increase on uniform surfaces[20] is limited by a multiplicative factor of $4^{2/3}$, which was shown to be in close agreement with the experimentally observed maximum increase in film thickness on a fiber by Carroll and Lucassen.[30] The exponents of this factor and of the limiting factor in the present case are equal to the exponents of $\mathsf{Ca}$ in Eqs. (1) and (2), respectively. Detailed experiments on the thickness of surfactant solutions dip coated onto patterned surfaces do not yet appear in the literature, which precludes a direct comparison with the present analysis.

### B. Immobile interface limit

A limiting case considered for homogeneous surfaces is based on treating the free surface of the film as immobile due to a concentrated surfactant monolayer. Bretherton[23] used this condition to assess the effect of surfactant on the thickness of the film deposited by the motion of a long bubble in a cylindrical tube. In that work, the film thickness was found to be $2^{2/3}$ times greater than that in the case of a pure fluid, for which the interface is stress-free. The same factor was observed by Shen *et al.*[31] for the dip coating of a surfactant solution onto a fiber.

This immobile interface condition can also be applied to the dip coating of a micropatterned surface. In this case the concentration becomes uniform throughout the transition region, so that $\bar{\Gamma}=\bar{\Gamma}_{\bar{x}}=0$. The boundary condition given by Eq. (29) is replaced by a no-slip boundary condition at the free surface of the film. The differential equation governing the film thickness for this case reduces to

$$(\bar{h}_{\bar{x}\bar{x}\bar{x}} - \bar{h}_{\bar{x}}) = \frac{6(\bar{h} - \bar{h}_\infty)}{\bar{h}^3}. \tag{42}$$

The initial condition and the matching condition remain the same as for the previous case. Solving this equation in the similar manner gives $\bar{h}_\infty = 1.270\ 38$, which is exactly $2^{1/3}$ times more than the base case ($\mathsf{M}=0$) for a stress-free interface. Note also that Eq. (42) reduces to Eq. (32) for $\mathsf{M}=0$ with the rescaling $\hat{h}=2^{-1/3}\bar{h}$. Then $\bar{h}_\infty = 2^{1/3}\hat{h}_\infty$, with $\hat{h}_\infty = 1.008\ 29$. This analysis demonstrates that the Marangoni stresses can have more significant effects on the coating process than would be expected by assuming that the interface is rigid.

## V. DISCUSSION

The effect of surfactant on the deposited film thickness has previously been observed in many experimental and theoretical studies of uniform surfaces, including studies of the motion of a bubble in a capillary tube,[23,24] coating of a cylindrical fiber,[17,30] and coating of flat plates.[20,32] The dip coating of chemically patterned surfaces follows the same qualitative trends, although the magnitude of the film thickening due to Marangoni stresses is predicted to differ due to the effects of transverse fluid confinement by chemical patterning. In particular, the analysis in the present work reveals that the presence of insoluble surfactant can increase the thickness of the liquid film dip-coated onto chemically patterned surfaces in a nontrivial manner. Withdrawal of the plate from the liquid bath causes dilation of the free-surface, which decreases the concentration of surfactant in the entrained film relative to the liquid bath. This concentration gradient creates a gradient in surface tension, which induces a shear stress at the free surface. The resulting Marangoni flow from the meniscus to the deposited film results in film thickening relative to the case of a pure liquid. The trend for dimensionless full thickness versus $\mathsf{Ca}$ is qualitatively similar to the case of a uniform substrate, and the maximum effect on the thickness of the entrained film occurs for a value of $\mathsf{Ca}$ intermediate to the range considered. For a particular value of $\mathsf{M}$, there is an increase in film thickness with $\mathsf{Ca}$ until $\mathsf{Ca} \approx 10^{-8}-10^{-5}$, depending on the value of $\bar{D}$. After that transition, there is a decrease in the film thickness with increasing values of $\mathsf{Ca}$.

At values of $\mathsf{Ca}$ below the transition, surface diffusion becomes significant and smooths the concentration profile, which reduces the Marangoni stress. An increase in $\mathsf{Ca}$ in this regime decreases the surface concentration of the surfactant in the film because surface diffusion cannot fully compensate for the surface dilation caused by the plate motion. The resultant surfactant gradient induces a Marangoni flow that increases the thickness of the entrained film. Note that for $D_s=0$, this lower transition does not occur, as shown in Fig. 2. For larger values of $\mathsf{Ca}$ above the transition point, the Marangoni flow is overwhelmed by the viscous forces due to the plate motion, so the thickening factor decreases for that particular value of $\mathsf{M}$ as $\mathsf{Ca}$ increases further. Analogous trends are predicted for film deposition on uniform surfaces,[20,24] and this decrease in thickening factor with increasing $\mathsf{Ca}$ has been observed experimentally.[17,23,33]

The effect of increasing $\mathsf{Ca}$ can be clearly seen from the concentration profiles shown in Fig. 7, which were computed for the intermediate value $\mathsf{M}=0.01$. The figures correspond to the concentration profiles of the surfactant for $\mathsf{Ca}=10^{-3}$ and $\mathsf{Ca}=10^{-6}$ (inset). As $\mathsf{Ca}$ increases, the profiles tend to get steeper, and $\bar{\Gamma}_c \to -1$, which corresponds to no surfactant on the entrained film. Also, with increasing $\mathsf{Ca}$, the concentration profiles for different values of $W$ tend to overlap, showing the dominant effect of the motion of the plate to the dip coating process. The surfactant concentration on the entrained liquid film, $\bar{\Gamma}_c$, allows a calculation of the transfer efficiency of surfactant from the bulk liquid to the deposited film, which may be of interest for many applications related to Langmuir-Blodgett films.[34,35]

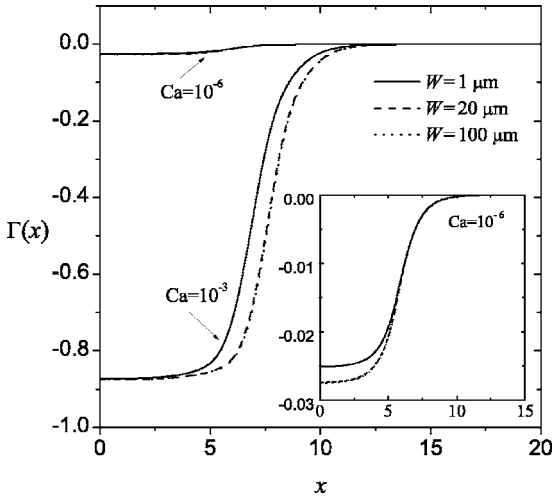


FIG. 7. Dimensionless surfactant concentration profile $\Gamma(x)$ for $\mathrm{Ca}=10^{-3}$ and $\mathrm{Ca}=10^{-6}$ (inset). The curves for $W=20$ $\mu$m and $W=100$ $\mu$m cannot be distinguished on the scale of the plot.

## VI. SUMMARY AND CONCLUSIONS

The effect of insoluble surfactant on the dip coating of chemically micropatterned surfaces has been theoretically investigated via a matched asymptotic analysis of equations derived using lubrication theory. The increase in the thickness of the deposited liquid film (due to Marangoni stresses) relative to a pure liquid is limited by a multiplicative factor of $4^{1/3}$, which is $2^{1/3}$ times larger than predicted if the liquid-vapor interface is assumed immobile due to the presence of a concentrated surfactant monolayer. The maximum increase is $4^{1/3}$ times less than for a homogeneous surface, which is due to the Ca dependence imposed by the transverse curvature of the free surface caused by lateral fluid confinement by substrate micropatterning. The maximum effect of Marangoni stresses occurs for a value of Ca intermediate to the range considered in this analysis because surface diffusion and viscous stresses dominate at smaller and larger values of Ca, respectively, and the results for a pure liquid are recovered in these limits. Both the thickness of the deposited liquid film and concentration of the deposited surfactant monolayer are determined for a wide range of capillary numbers, stripe widths, and Marangoni factors relevant to the numerous applications of dip coating on chemically micropatterned surfaces.

## ACKNOWLEDGMENT

J.M.D. gratefully acknowledges support from a 3M Nontenured Faculty Award.

[1] A. A. Darhuber, S. M. Troian, J. M. Davis, S. M. Miller, and S. Wagner, "Selective dip coating of chemically micropatterned surfaces," J. Appl. Phys. **88**, 5119 (2000).
[2] P. R. Schunk, A. J. Hurd, and C. J. Brinker, in *Liquid Film Coating*, edited by S. F. Kistler and P. M. Schweizer (Chapman & Hall, London, 1997).
[3] D. Qin, Y. Xia, B. Xu, H. Yang, C. Zhu, and G. M. Whitesides, "Fabrication of ordered two-dimensional arrays of micro- and nanoparticles using patterned self-assembled monolayers as templates," Adv. Mater. (Weinheim, Ger.) **11**, 1433 (1999).
[4] D. A. Doshi, A. Gibaud, N. Liu, D. Sturmayr, A. P. Malanoski, D. R. Dunphy, H. Chen, S. Narayanan, A. MacPhee, J. Wang, S. T. Reed, A. J. Hurd, F. van Swol, and C. J. Brinker, "In-situ x-ray scattering study of continuous silica-surfactant self-assembly during steady-state dip coating," J. Phys. Chem. B **107**, 7683 (2003).
[5] H. Y. Fan, Y. F. Lu, A. Stump, S. T. Reed, T. Baer, R. Schunk, V. Perez-Luna, G. P. Lopez, and C. J. Brinker, "Rapid prototyping of patterned functional nanostructures," Nature **405**, 56 (2000).
[6] H. G. Braun and E. Meyer, "Thin microstructured polymer films by surface-directed film formation," Thin Solid Films **345**, 222 (1999).
[7] S. J. Oh, Y. Cheng, J. Zhang, H. Shimoda, and O. Zhou, "Room-temperature fabrication of high-resolution carbon nano-tube field-emission cathodes by self-assembly," Appl. Phys. Lett. **82**, 2521 (2003).
[8] H. Ko, S. Peleshanko, and V. Tsukrut, "Combing and bending of carbon nano-tube arrays with confined microfluidic flow on patterned surfaces," J. Phys. Chem. B **108**, 4385 (2004).
[9] V. Santhanam and R. P. Andres, "Microcontact printing of uniform nanoparticle arrays," Nano Lett. **4**, 41 (2004).
[10] Q. Guo, X. Teng, S. Rahman, and H. Yang, "Patterned Langmuir-Blodgett films of monodisperse nanoparticles of iron oxide using soft lithography," J. Am. Chem. Soc. **125**, 630 (2003).
[11] L. D. Landau and B. V. G. Levich, "Dragging of a liquid by a moving plate," Acta Physicochim. URSS **17**, 42 (1942).
[12] B. M. Deryagin and S. M. Levi, *Film Coating Theory* (Focal, New York, 1964).
[13] D. A. White and J. A. Tallmadge, "Theory of drag out of liquids on flat plates," Chem. Eng. Sci. **20**, 33 (1965).
[14] C. Y. Lee and J. A. Tallmadge, "Description of meniscus profiles in free coating," AIChE J. **18**, 858 (1972).
[15] S. D. R. Wilson, "The drag-out problem in film coating theory," J. Eng. Math. **16**, 209 (1982).
[16] O. Reglat, R. Labrie, and P. A. Tanguy, "A new free-surface model for the dip coating process," J. Comput. Phys. **109**, 238 (1993).
[17] D. Quéré, "Fluid coating on a fiber," Annu. Rev. Fluid Mech. **31**, 347 (1999).
[18] S. J. Weinstein and K. J. Ruschak, "Coating flows," Annu. Rev. Fluid Mech. **36**, 29 (2004).
[19] J. M. Davis, "Asymptotic analysis of liquid films dip-coated onto chemically micropatterned surfaces," Phys. Fluids **17**, 038101 (2005).
[20] C.-W. Park, "Effects of insoluble surfactants on dip coating," J. Colloid Interface Sci. **146**, 382 (1991).
[21] A. Thess and W. Boos, "A model for Marangoni drying," Phys. Fluids **11**, 3852 (1999).
[22] O. K. Matar and R. V. Craster, "Models for Marangoni drying," Phys. Fluids **13**, 1869 (2001).
[23] F. P. Bretherton, "The motion of long bubbles in tubes," J. Fluid Mech. **10**, 166 (1961).
[24] J. Ratulowski and H. C. Chang, "Marangoni effects of trace impurities on the motion of long gas bubbles in capillaries," J. Fluid Mech. **210**, 303 (1990).
[25] S. D. R. Wilson, "Coating flow on to rods and wires," AIChE J. **34**, 1732 (1988).
[26] L. L. Lo, "The meniscus on a needle—A lesson in matching," J. Fluid Mech. **132**, 65 (1983).
[27] E. O. Tuck and L. W. Schwartz, "A numerical and asymptotic study of some third-order ordinary differential equations relevant to draining and coating flows," SIAM Rev. **32**, 453 (1990).
[28] L. W. Schwartz, "On the asymptotic analysis of surface-stress-driven thin-layer flow," J. Eng. Math. **39**, 171 (2001).
[29] J. C. Berg and A. Acrivos, "Effect of surface active agents on convection cells induced by surface tension," Chem. Eng. Sci. **20**, 737 (1965).
[30] B. J. Carroll and J. Lucassen, "Capillarity controlled entrainment of liquid by a thin cylinderical filament," Chem. Eng. Sci. **28**, 23 (1973).
[31] A. Q. Shen, B. Gleason, G. H. McKinley, and H. A. Stone, "Fiber coating with surfactant solutions," Phys. Fluids **14**, 4055 (2002).
[32] L. Y. Zhang and M. P. Srinivasan, "Hydrodynamics of subphase entrainment during Langmuir-Blodgett film deposition," Colloids Surf., A **193**, 15 (2001).
[33] L. W. Schwartz, H. M. Princen, and A. D. Kiss, "On the motion of bubbles in capillary tubes," J. Fluid Mech. **172**, 259 (1986).
[34] K. B. Blodgett, "Films built by depositing successive monomolecular layers on a solid surface," J. Am. Chem. Soc. **57**, 1007 (1935).
[35] G. Roberts, *Langmuir-Blodgett Films* (Plenum, New York, 1990).